USGS Award Number: G11AP20005
Project Duration: 12 months

Final Technical Report

Continuation of Detection and Location of Non-volcanic Tremor in the New Madrid Seismic Zone

Heather R. DeShon[1], Charles A. Langston[1], Blaine Bockholt[1], Stephen P. Horton[1]

[1]Center for Earthquake Research and Information
University of Memphis
3876 Central Ave., Suite 1
Memphis, TN 38152-3050

(901) 678-1527, fax (901) 678-4734, hdeshon@memphis.edu
(901) 678-4869, fax (901) 678-4734, clangstn@memphis.edu
(901) 678-4896, fax (901) 678-4734, shorton@memphis.edu

Submitted on April 9, 2012

Abstract

Data from the existing Cooperative New Madrid Seismic Network and from a 2-year deployment of a high-frequency phased array were used to detect and locate non-volcanic tremor (NVT) recently discovered in the New Madrid Seismic Zone (NMSZ). *Langston et al.* (2010) originally hypothesize that NVT consists of temporally-energetic swarms of micro-earthquakes at the M_L -1 to -2 level occurring at mid-crustal levels in the NMSZ. Such events were serendipitously detected in November 2006 on a reflection/refraction experiment near the Reelfoot fault where hundreds of small events occurred in one afternoon. Due to its similarity to volcanic tremor, NVT in other environments has been associated with temporal variability in frictional and fluid-related processes. Microearthquake swarm activity along the NMSZ suggest that this intraplate system may also maintain spatial and/or temporal variability of fluid-related processes.

A high-frequency, phased array of 19 broadband seismic stations was deployed between November 2009 and September 2011 over the Reelfoot fault to detect NVT signals at ground motion levels equivalent to M_L -2. Array analysis increases signal-to-noise ratios and yields wave azimuth and slowness information that can be used to estimate locations for these small events. We also set up a network archiving protocol for the existing seismic network to record and process data from selected high-quality stations continuously over the time period of this project. The continuous network data was used to investigate temporal changes in background noise levels that might be due to increased NVT activity at depth. The temporal and spatial characteristics of NVT within the New Madrid fault system are critical parameters that potentially relate a seismic observable to strain within the fault zone. NVT occurring at deep levels in this intraplate fault zone may be related to ductile processes similar to those postulated for NVT in subduction zones and at deep levels of the San Andreas fault. NVT within shallower parts of the fault where typical microseismicity now occurs may reflect unusual brittle failure processes associated with stress heterogeneity or anomalous pore pressure states. Here, we present years 1 and 2 data from the array and report findings.

Introduction

One of the most exciting discoveries to be made within the New Madrid Seismic Zone (NMSZ) in recent years is the possibility that non-volcanic tremor may be occurring within this intraplate fault system (*Langston et al.*, 2010). A reflection/refraction experiment near Mooring, TN, recorded a sequence of high frequency signals that moved across the linear array at 3-25 km/s. The arrivals were not large enough to trigger the regional seismic network, and continuous seismic data were not archived from nearby stations. The signals could not be well located, but we note that the Mooring experiment was located above the downdip edge of microseismicity associated with the Reelfoot reverse fault. The signals recorded at the Mooring experiment were reminiscent of the packets of energy reported for non-volcanic tremor in subduction and strike-slip fault environments. We use the term "NVT" to represent a continuum of signals ranging from swarms of small overlapping or distinct earthquakes lasting days to noise-like tremor lasting minutes to days.

NVT is a relatively new phenomenon in fault dynamics that was originally coined to describe coherent noise or tremor signals related to subduction processes in southwest Japan (*Obara*, 2002). The signal has since been found to be associated with episodic slip recorded by GPS in the Cascadia subduction zone of the Pacific Northwest (*Rogers and Dragert*, 2003; *Dragert, et al., 2001*). Improved continuous seismic and GPS data has led to the identification of NVT and/or slow slip processes in subduction zones along Cascadia, Japan, New Zealand, Mexico, and Costa Rica (e.g., *Schwartz and Rokosky*, 2007), Taiwan (*Peng and Chao*, 2008), and at deep levels of the San Andreas fault in central California (e.g., *Nadeau and Dolenc*, 2005; *Shelly,* 2010). Frictional stability arguments would suggest that the transition from stick-slip (velocity strengthening) to aseismic (velocity weakening) may pass through the conditional stability regime in a fairly heterogeneous fashion (e.g., *Scholz*, 1998). Models of tremor based on rate-and-state friction indicate that tremor may arise as seismogenic zone boundary phenomena in the presence of fluids (*Liu and Rice*, 2005; 2007), and, as such, NVT may not be limited to plate boundary faults. Recent studies show that tremor can be modulated by teleseismic and tidal signals (*Nakata et al.*, 2008; *Rubenstein et al.*, 2007, 2008; *Peng et al.*, 2008, 2009; *Ghosh et al.*, 2009) and in some cases is composed of overlapping shear failures (*Shelly et al.*, 2006; *Brown et al.*, 2008, *Maceira et al.*, 2010). NVT may represent failure of critically stressed faults with near lithostatic pore fluid pressures (*Thomas et al.*, 2009).

Our target for this project was to re-identify and find the spatial and temporal location of NVT and other seismic signals, such as swarms, that have been identified within the NMSZ. Our working hypothesis was that intense swarms of very small micro-earthquakes ($M_L < 1$) occur regularly within the NMSZ and were associated with strain processes on shallow and deep boundaries of the seismogenic segments of New Madrid faults. We targeted the Reelfoot Fault, the central reverse fault associated with the NMSZ. There are two major data collection tasks: (1) the installation and data collection associated with the phased array and (2)

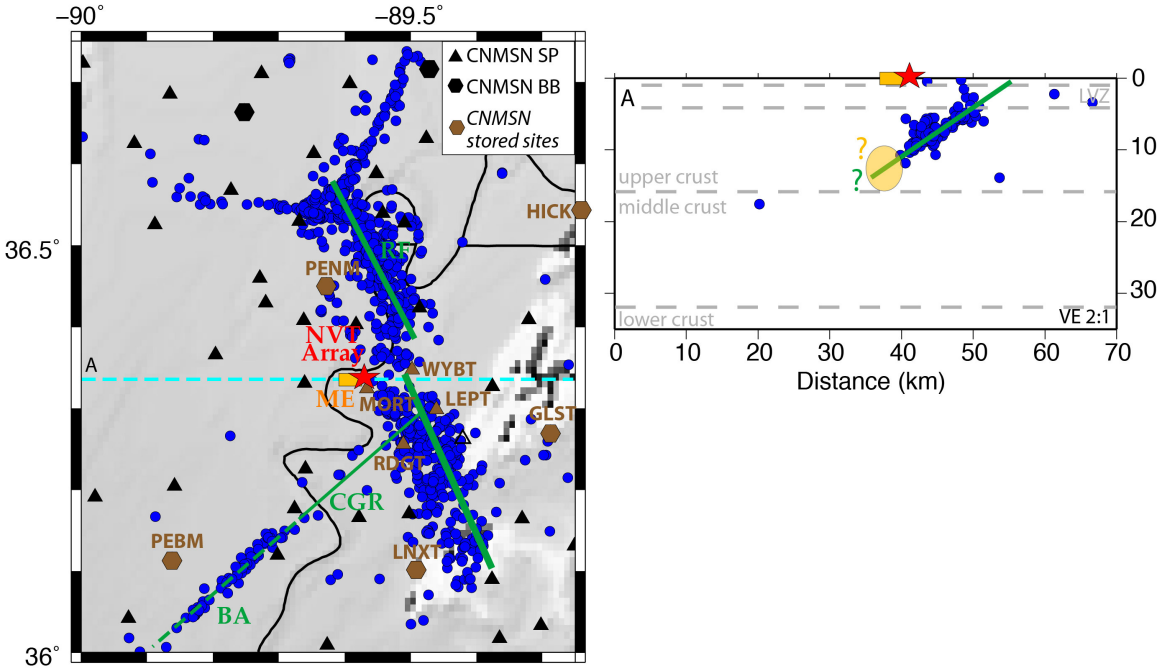

Figure 1: (left) Map of the New Madrid Seismic Zone. Microseismicity delineates four primary structures including the Reelfoot reverse fault (RF) and the Cottonwood Grove/Blytheville Arch lineation (CGR/BA). Seismicity is recorded by short-period and broadband stations (black triangles and hexagons) associated with the Cooperative New Madrid Seismic Network (CNMSN). Stations being stored in continuous mode as part of this experiment are shown in brown. Red star: current phased site; Orange rectangle: The Mooring experiment; Dotted cyan line show cross-section location shown at the right. (right) Cross-sections are taken through the NVT array and Mooring Experiment (A). The orange ellipse represents the hypothesized location for signals recorded by the Mooring experiment based on moveout curves.

reprogramming of permanent network data protocols to allow for continuous data storage. A 19-station phased array was deployed in November 2009 using instrumentation from the IRIS PASSCAL Instrument Center (Fig. 1, red star). The array was constructed and located to detect high phase velocity P and S waves from the NVT. The array remained in place until September 2011. Data from nine short-period and broadband Cooperative New Madrid seismic network stations (Fig. 1, brown hexagons) were continuously stored, processed using tremor detection algorithms developed for subduction zone NVT studies, and used to identify and relocate local earthquakes recorded on the array. Results are discussed below.

The NVT Array

NVT is a basic observation that can help understand the dynamics of a fault zone. Tremor sources are difficult to locate because they generally do not have distinct P and S wave arrivals (*Wech and Creager,* 2007). Although tremor sources can be approximately located using envelope time-distance moveout across a network for

major peaks in the time series, small aperture, phased arrays offer a superior way to detect and provide far more precise locations of deep non-volcanic tremor. A phased array is capable of directly measuring the phase velocity of the wavefield at any moment in time through conventional plane wave slowness analysis. The measured slowness vectors can be used to constrain event locations (e.g. *Pavlis et al.*, 2004; or *Eagar et al.*, 2006). The 19-element phased array was constructed and located to detect high phase velocity P and S waves from the NVT. Using a phased array significantly increases signal-to-noise levels and provides horizontal slowness and azimuth estimates to locate the source of NVT.

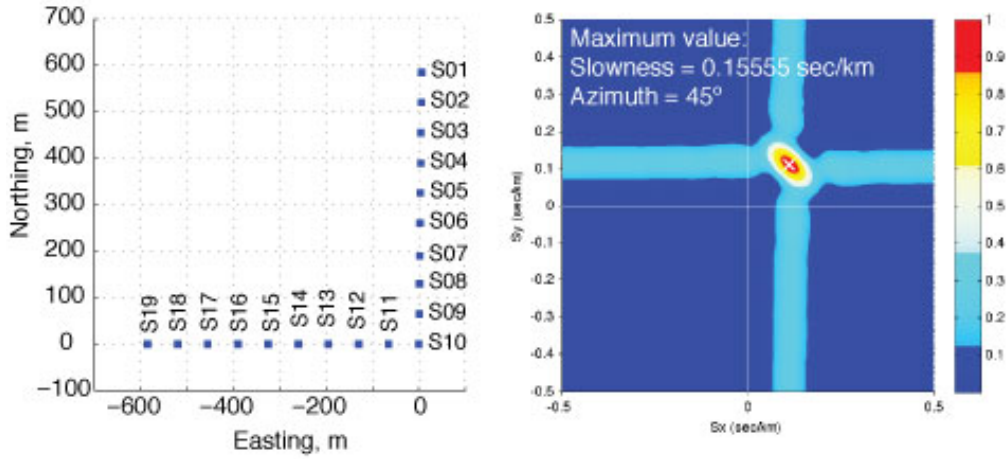

Figure 2: (left) Geometry of the high-frequency, phased array installed near Mooring, TN. The 19 element array is arranged in an L-shape to take advantage of the available field. (right) Theoretical broadband frequency/wavenumber response for a plane wave with a slowness of 1/6 sec/km, an azimuth of arrival of 45º, and bandwidth between 10-20 Hz. The "L" geometry of the array causes the peak to be elongated in the NW/SE direction with some elongated sidelobes in the NS and EW directions.

The NMSZ is located under an extensive blanket of thick (up to 1 km) unconsolidated sediments of late Cretaceous, Tertiary, and Quaternary age. These sediments represent a challenge for clear recording of microearthquakes and NVT. These sediments cover a complex and deformed Paleozoic section of possibly 7 km deep rift basins of the Reelfoot rift (*Dart and Swolfs*, 1998; *Ervin and McGinnis*, 1975; *Stearns*, 1957; *Stearns and Marcher*, 1962; *Thomas*, 2006). The Paleozoic basement/ sediment interface creates large S-to-P converted phases that can be misidentified as S waves (e.g., *Andrews, et al.*, 1985; *Langston*, 2003). Thus, 3-component recording is a must to discriminate between P and S waves. Sediments of the embayment also amplify ambient ground motions compared to sites on more competent rock outside of the embayment (*Jemberie and Langston*, 2005) and also act as an efficient high frequency waveguide that can produce high amplitude body and surface waves (*Langston et al.*, 2005; 2006). Increased noise levels also tend to mask signals from small events. Array recording is necessary to increase signal-to-noise ratios for natural seismicity and to discriminate and identify seismic phases on the basis of their horizontal phase velocities and particle motions. The

combination of relative P and S arrival times, azimuth and horizontal slowness measurements enables an estimate of the location of events.

ARRAY DESIGN AND RESPONSE

The 19-station high-frequency, phased array was deployed in northwestern Tennessee in the region of the Mooring Experiment (Fig. 1, Table 1). It was difficult to find large, unused fields in the vicinity of the Reelfoot Fault to install an areally-distributed array. The natural geometry was to use the edge of a large farm field to site array elements in order to cut down on land usage costs and improve the logistics of installation and servicing at the expense of a somewhat degraded array response (Fig. 2). The array was used to search for coherent tremor signals propagating across the array and greatly improves signal to noise ratio for very small events. Figure 2 shows the array geometry and the theoretical broadband f-k response (10-20 Hz) for a wave arriving at 45 degrees azimuth with a phase velocity of 6 km/s. The required "L" geometry of the array causes the peak to be elongated in the NW/SE direction with some elongated sidelobes in the NS and EW directions.

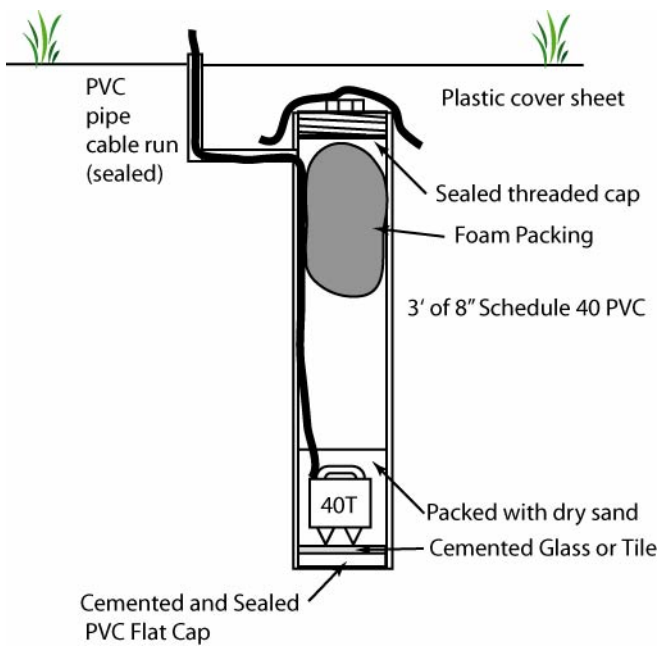

Figure 3: Schematic station installation design. Each sensor is placed in a 4 ft mini-borehole, packed with dry sand, and insulated.

We installed PASSCAL equipment consisting of CMG-40T seismometers, Reftek-130 DAS's, and solar panels (Fig. 3). Continuous data were collected from flash drives in the field every ~8-16 weeks, quality controlled, and sent to the IRIS Data Management Center for archiving. Data from station S10 was made available at this time, while the remaining 18 stations remained under 2-year proprietary usage, set to expire Sept. 2013. All data covering the report period (Nov. 2009 – Sept. 2011) have been archived with the DMC under network code Y8 (Fig. 4). CMG-40T sensors

were the appropriate choice here for three reasons. First, they are less subject to the long experimental delays in requests for sensors with a wider recording bandwidth. Second, the bandwidth of this sensor is more than adequate for this experiment (10 or 30 s to 100 Hz). Finally, the noise level in this area is high enough that higher sensor noise level is not a factor. All sensor and data acquisition changes are correctly recorded in metadata at the DMC. Table 1 lists the station locations.

Flooding in 2010 and 2011

In general, maintenance was minimal, and data quality very high. However, the study area experienced historic flooding events in May of 2010 and 2011. End stations S01, S18, and S19 lost data during the extreme regional flooding event of May 2010 (Julian days 122-202). In 2011, flooding reached historic levels along the Mississippi river, and we feared the levee located near the array would fail. We

Table 1: Station Locations

Station	Latitude	Longitude	Elevation(km)	Easting(m)*	Northing(m)*
S01	36.3190	-89.5326	0.089	0	540
S02	36.3184	-89.5327	0.087	0	480
S03	36.3178	-89.5327	0.087	0	420
S04	36.3173	-89.5327	0.088	0	360
S05	36.3166	-89.5327	0.088	0	300
S06	36.3160	-89.5327	0.088	0	240
S07	36.3154	-89.5327	0.087	0	180
S08	36.3149	-89.5328	0.088	0	120
S09	36.3143	-89.5328	0.087	0	60
S10	36.3137	-89.5328	0.087	0	0
S11	36.3137	-89.5335	0.088	-60	0
S12	36.3137	-89.5343	0.087	-120	0
S13	36.3137	-89.5350	0.087	-180	0
S14	36.3137	-89.5357	0.087	-240	0
S15	36.3137	-89.5364	0.088	-300	0
S16	36.3138	-89.5371	0.088	-360	0
S17	36.3138	-89.5379	0.087	-420	0
S18	36.3138	-89.5386	0.086	-480	0
S19	36.3138	-89.5393	0.087	-540	0
GLST	36.2692	-89.2877	0.122		
LEPT	36.2985	-89.4607	0.066		
MORT	36.3247	-89.5662	0.083		
WYBT	36.3477	-89.4975	0.082		
RDGT	36.2562	-89.5110	0.081		
HICK	36.5408	-89.2288	0.141		
LNXT	36.1013	-89.4913	0.144		
PEBM	36.1132	-89.8623	0.076		
PENM	36.4502	-89.6280	0.085		

*Array stations approximate to center station S10.

decided to remove all surface instrumentation susceptible to water (REF-TEKs, power boards, etc.) but left the sensors in the ground. As a result, there is no data recovery between April 28 and May 17, 2011 (Julian days 118-137) (Fig. 4). Sensors at S19 and S16 were damaged during this flooding event and while they continue to report bits, the data became useless for the remainder of the experiment.

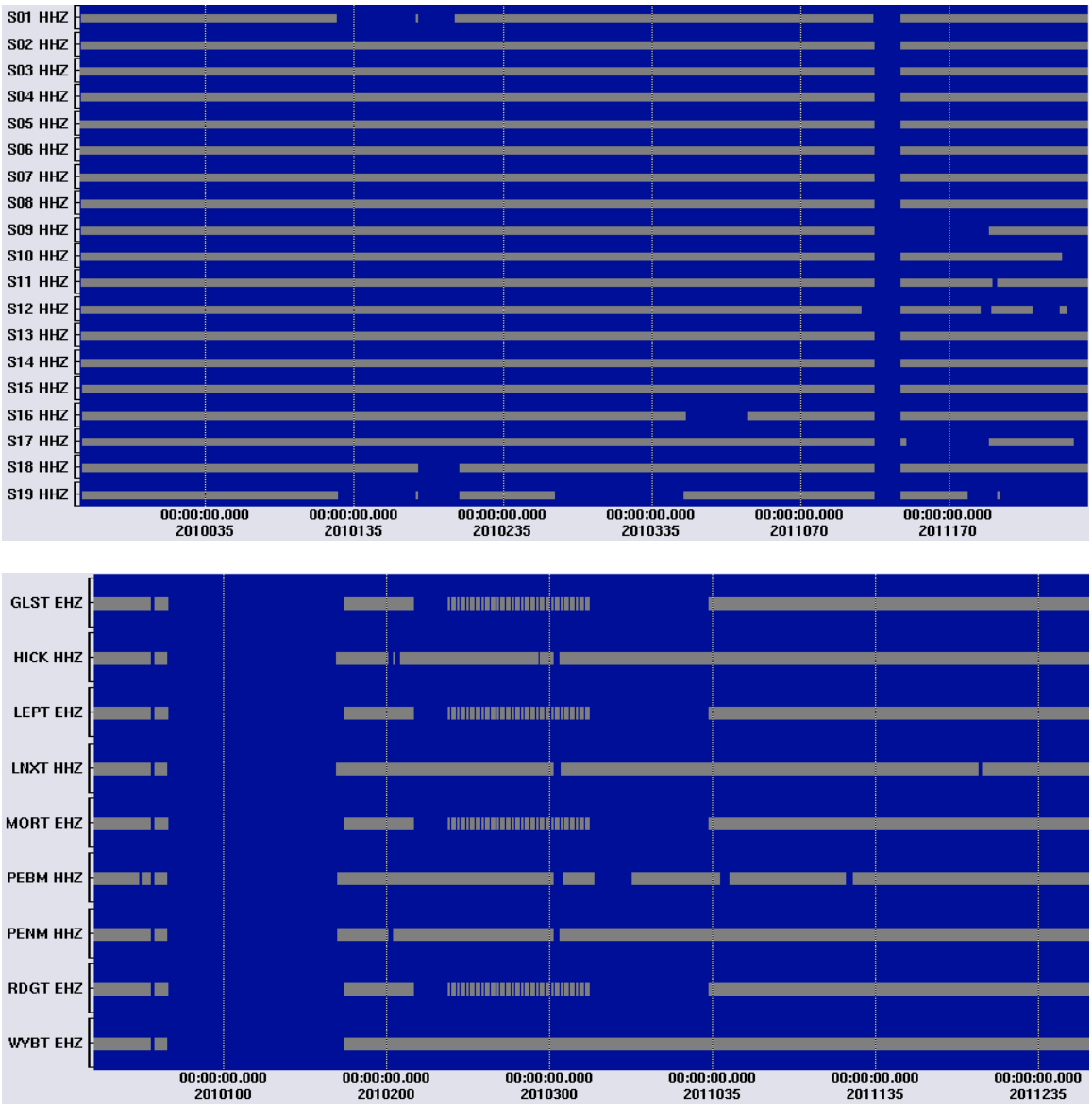

Figure 4: Data archive and storage history for the NVT array continuous data (top) and selected permanent network stations (bottom). The gray shading shows data availability for the project period covered by this report. Note that only vertical channel data are shown but all components have identical data availability.

Permanent Network Data

Continuous recordings for nine CNMSN broadband and short-period stations located near the NVT array have been stored under this award (Fig. 1, Table 1). Storage required the completed installation and testing of CNMSN upgrades to data transfer protocols and a creation of an experiment specific waveserver at the network communication node LNXT. Once in place, we were able to begin storage of continuous data in the form of miniseed day volumes (Fig. 4, bottom). Technical problems with the new data transfer protocols and our automated storage scripts contributed to a significant loss of stored data for this experiment in mid-2010. These problems have since been overcome, as evidenced by the improved data recovery. Storage of broadband data (HICK, LNXT, PENM, PEBM, and WYBT) was more consistent then the short-period data (GLST, LEPT, MORT, RDGT).

Array and limited permanent network data were integrated into an Antelope database, which allowed for automatically detecting arrivals and associating local earthquakes to the CERI catalog. The STA/LTA autodetector *dbdetect* identifies local, regional, and teleseismic events, but also returns a large number of false identifications. The catalog therefore has to be reviewed manually by an analyst to remove "events" that are not earthquakes.

The array and network recorded many significant earthquakes and seismic signals, which could be used for allied studies. Teleseismic events include the Mw 7.0 Haiti, Mw 8.8 Maule Chile, and Mw 9.0 Tohoku-Oki earthquakes; regional events with M>3.8 in Arkansas, Colorado, Illinois, Oklahoma and Virginia were also recorded (Fig. 5). The array recorded a series of airgun shots along the Mississippi River in summer 2010 (Fig. 6). The array data combined with the continuous CNMSN waveforms and pick catalog will be an excellent dataset for a range of local earthquake studies and it may prove useful to look for triggered seismicity along the Reelfoot Fault. Triggered microseismicity and triggered tremor have been reported along the San Andreas Fault (e.g., *Peng et al.*, 2008,2009; *Thomas et al.*, 2009), and we continue to explore the possibility that either microseismicity or NVT signals could be triggered in the NMSZ.

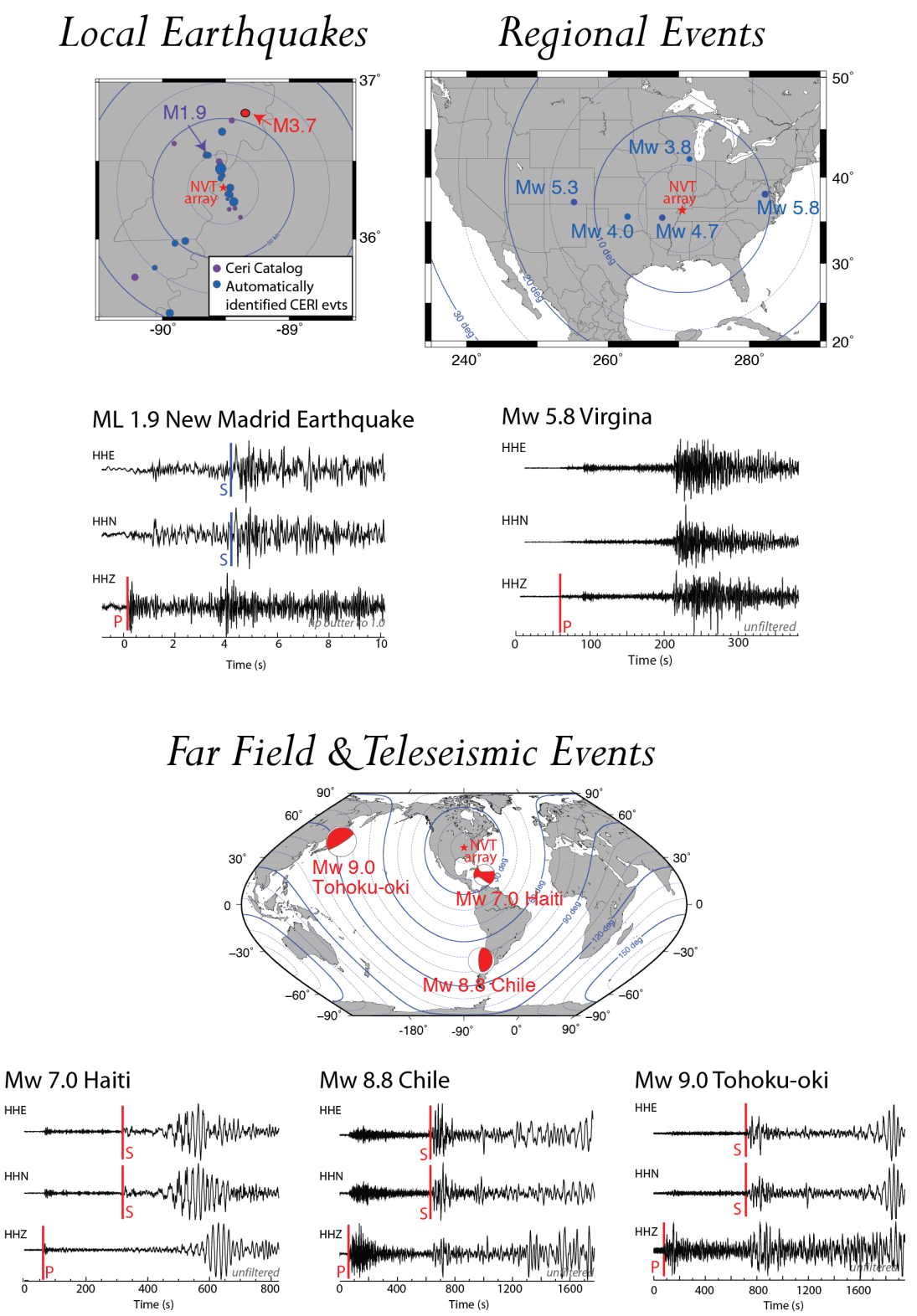

Figure 5: Example waveforms from station S10 of local, regional, far field and teleseismic earthquakes recorded by the NVT array. Data quality is excellent.

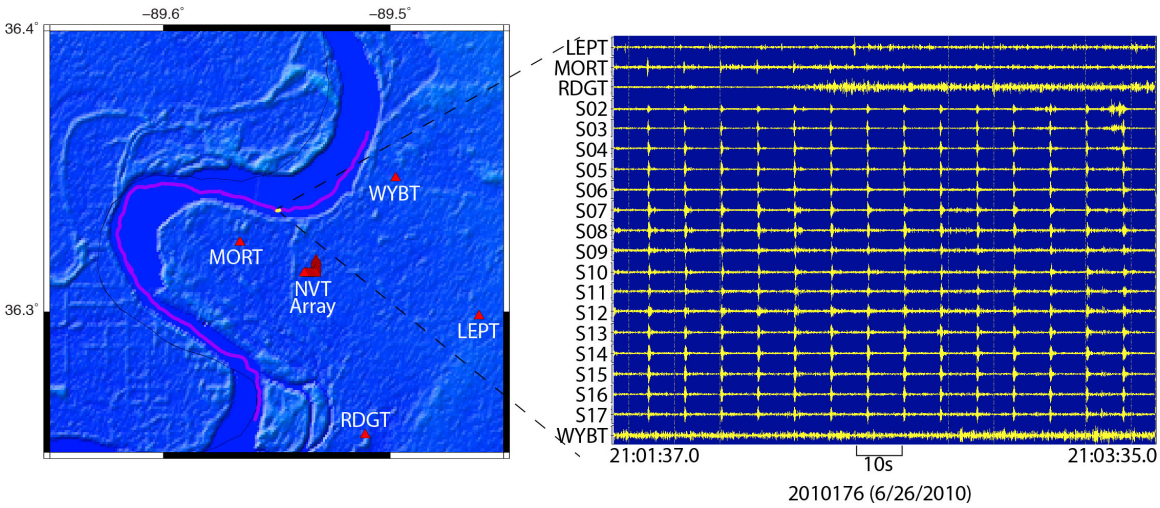

Figure 6: Recordings of shots fired along the Mississippi River in 2010 as part of the Mississippi Moonwalk Project (Magnani and McIntosh, personal communication 2010). Shown are vertical component recordings of the broadband array data and the near-by short-period CNMSN stations filtered between 8-15 Hz. We have found shots were well-recorded on 6/25-26/2010, as the boat traveled along the purple line shown to the left.

Significant Results

ABILITY TO RESOLVE SMALL SIGNALS

We used the BroadBand frequency/wavenumber (BBFK) method of *Nawab et al.* (1985) to analyze the array data without any corrections for individual array element site structures. Figure 7 shows the BBFK result for 20 s of low-amplitude, oscillatory signal that is comparable in amplitude to signals seen in the discovery data of possible non-volcanic tremor from the Reelfoot Fault in 2006. This demonstrated that the array was sensitive enough to detect similar, possible NVT, in the future. However, the character of the signal in Figure 7 was quite different, showing periodic behavior and oscillatory motions. The array response shows two main sources of these waves to the NW and to the North. The apparent velocity is approximately 2 km/s and is consistent with the sediment-trapped P wave that is the dominant high-frequency phase seen in explosion data (*Langston et al.*, 2005). This noise source is likely from farm machinery or pumping and consists of acoustic waves propagating in the unconsolidated sediments of the embayment. The configuration and sensitivity of the array was sufficient to detect signals of the size seen in the discovery data set.

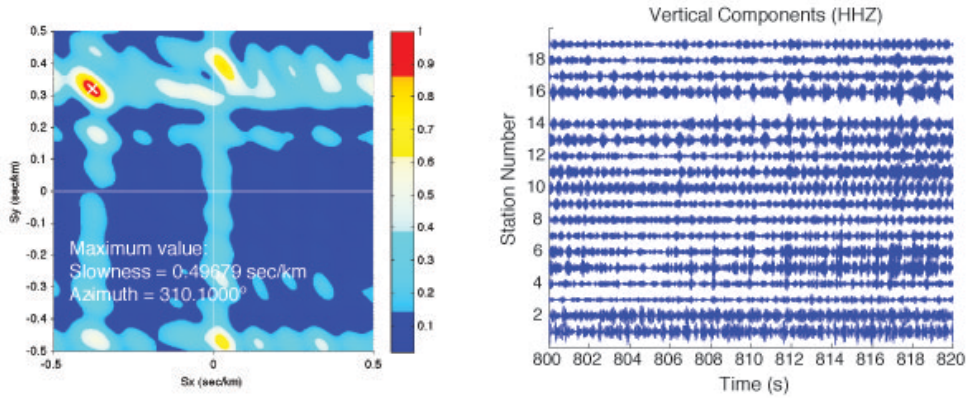

Figure 7: (left) Frequency/wavenumber response for background noise filtered between 10-20 Hz. (right) Plot of the filtered background noise used for BBFK analysis. An oscillatory, ambient noise signal was detected. These signal levels are comparable to those seen in the discovery data of possible non-volcanic tremor from the Reelfoot Fault in 2006 and demonstrate that the array was sensitive enough to detect similar possible NVT in the future.

However, the array responses for the observed signals (Fig. 7) show the effect of multipathing that produces the irregular character of the side-lobes compared to the theoretical response shown in Figure 2. Analysis of P and S wave signals from small local earthquakes (not shown) also demonstrated that waves are not purely coherent at these high frequencies across the array. It is likely that the near-surface layer, which is about 10 m thick in this area (*Langston*, 2003), is variable across the array and that array deconvolution techniques (e.g., *Der et al.*, 1987) could be used to improve the array response in future work.

LOCAL SEISMICITY RATE

We have manually reviewed ~1 year of autodetected events. During that time period, we have identified over 400 local earthquakes (Fig. 8), excluding events related to ongoing swarm activity in Arkansas. We identify local earthquakes at a rate ~2.6 times higher than the CERI event catalog (Fig. 8b), but many of the newly identified events are too small to be well-recorded by neighboring short-period CNMSN stations and are poorly located when only array stations are used. We record all 115 CERI catalog earthquakes during the reviewed time period and find an additional 308 earthquakes with clear P, Sp and S arrivals. The events are very small, must be located near to the array, and hence likely occur along the Reelfoot fault. Peaks in the number of events per week may be due to swarm activity or foreshock/ aftershock sequences (Fig. 8b). Bisrat et al. (2012) reported recurrent swarms near Ridgely, TN, which is located just to the southeast of the array, and we may have captured one or more such swarm events. Waveforms for events associated with rate increases in late 2011 were visually highly similar and event time separation was on the order of minutes to hours.

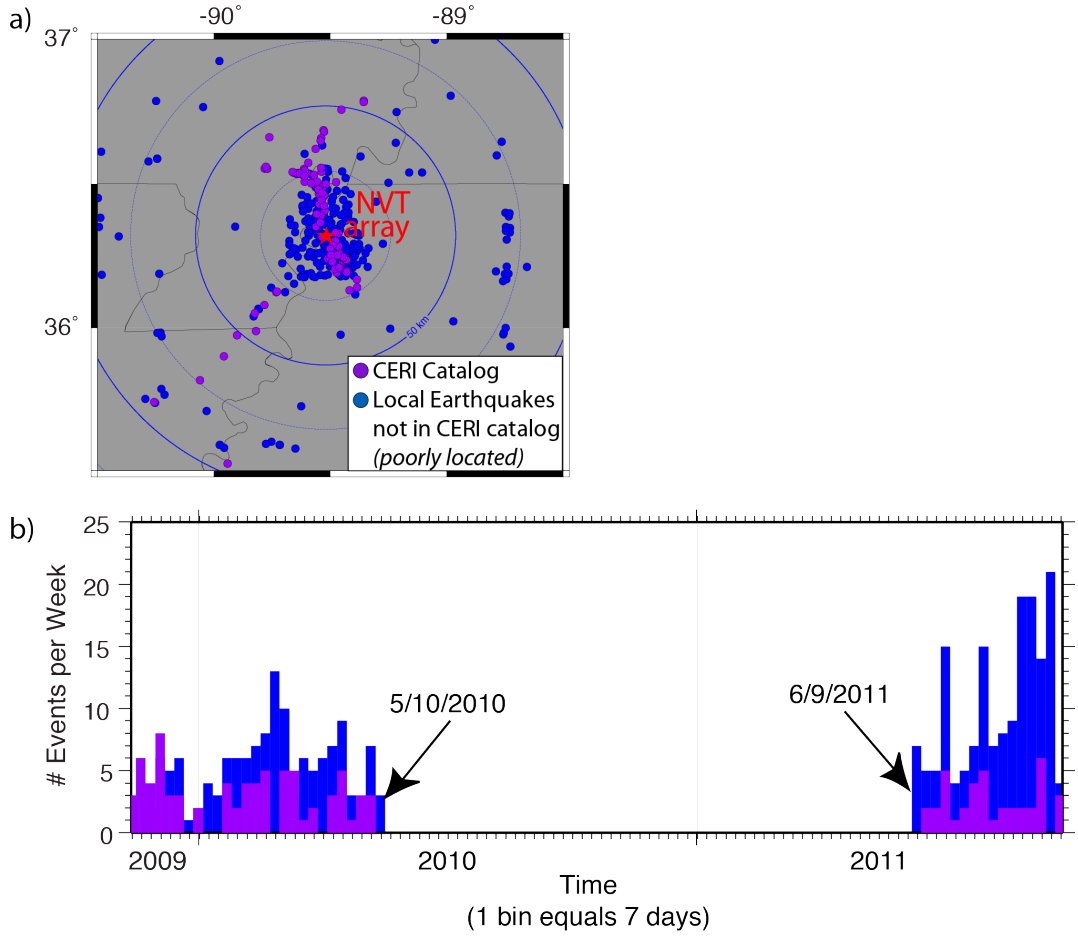

Figure 8: a) CERI catalog locations (purple) and newly identified local earthquakes recorded on the NVT array (blue). The newly identified earthquakes are poorly located, and only events occurring during the manually reviewed time period (Sept. 2009-May 10, 2010; June 9, 2011-Sept. 2011) are shown. b) Histogram showing number of events recorded per week in the CERI catalog (purple) and the NVT catalog (blue). The NVT array records all CERI catalog earthquakes; the blue histogram only reflects earthquakes not found in the CERI catalog.

BROADBAND FK ANALYSIS OF A LOCAL EARTHQUAKE

We have conducted BBFK analysis on a M3.7 earthquake recorded by the array (See Figure 5 for location). The waveforms are typical for NMSZ earthquakes, showing a large Sp conversion on the vertical component generated at the base of the unconsolidated sediment-basement interface, here about 700m under the array (Fig. 9). The extremely low velocity of near-surface material is evident from the lack of P wave motion on the horizontal components. The expected azimuth to the source based on the network location is 17º. BBFK results for the P waveforms indicated that the array response maximum is over 30º away from the expected azimuth (Fig. 9, top). The response also shows considerable multipathing. These waves can be

seen in the moveout of various wavelets behind direct P in the data. The source of multipath arrivals is likely due to variations in the velocity structure of the upper few meters across the array. For NS S-waves, the wavefield is much more complicated, and array response shows considerable evidence of multipath S-wave arrivals (Fig. 9, bottom). Low-pass filtering the EW S-wave data shows a remarkable succession of S wave reverberations in the sediment column.

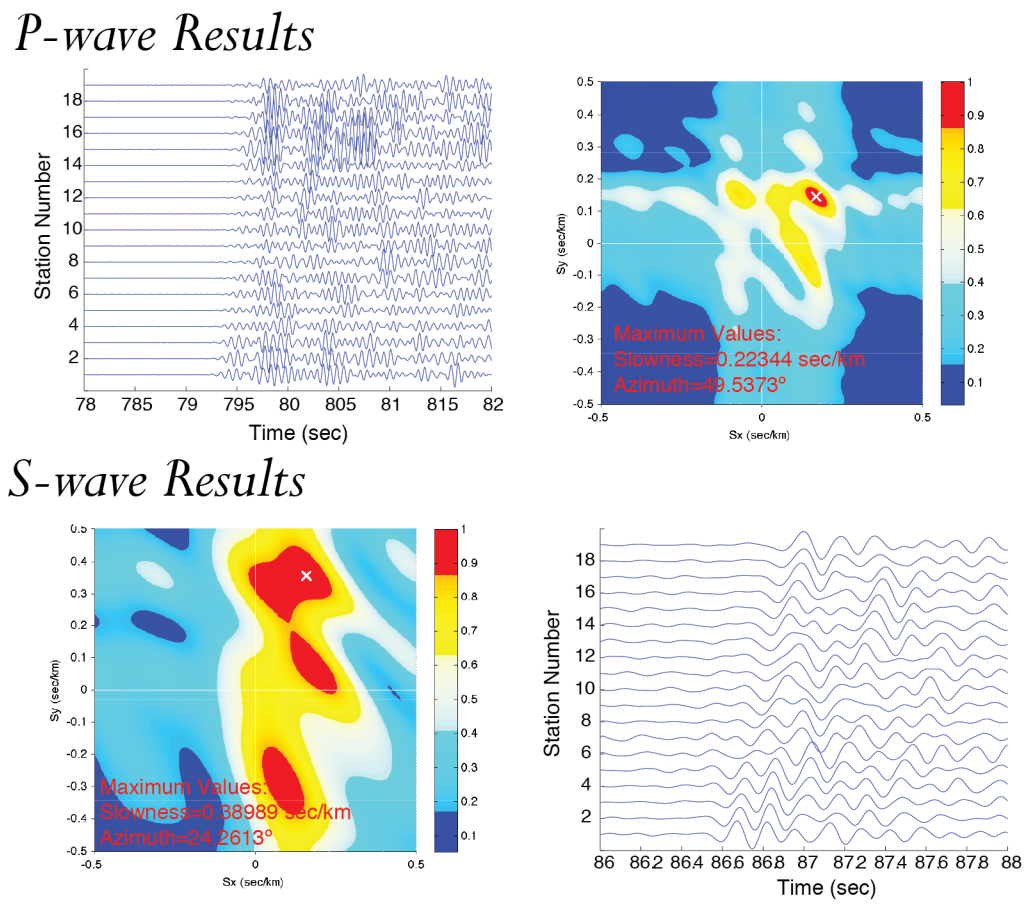

Figure 9: (top) BBFK results (right) using filtered P waveforms (left) for the M3.7 earthquake. (bottom) BBFK results (left) using filtered NS S waveforms (right).

AUTOMATED PROCESSING OF ARRAY DATA USING BBFK

We have investigated a number of techniques to pick out possible NVT from background noise using the character of the array response from local earthquakes and the character of the events seen in the discovery data set. Events seen in the discovery data set had high apparent velocities that were greater than 3km/s and phase move-outs that indicated a source region to the west. They were also best seen in the 8-15 Hz frequency band. Thus, we looked for similar high frequency arrivals in the array data set. It becomes important to examine the array response to incident P and S waves from local earthquakes, as done above, and to have some knowledge of the ambient seismic noise field to be able to discriminate between sources of seismic signals.

A straightforward way of approaching this problem is to examine short, consecutive array beams and look at the distribution of azimuth and slowness for the largest peak in the beam within the 8-15 Hz frequency band. After numerous attempts to determine the best search algorithm parameters for this large data set, we were able to maximize efficiency and minimize computational time using 10 second time windows with a 50% overlap. The data is preprocessed using a 5% cosine taper, bandpass filtered between the aforementioned 8-15 Hz and finally passed through the BBFK tools. To distinguish between the background and a signal of interest we again utilize the BBFK diagram. Figure 10 shows a 10 second time window of ambient noise and a coherent signal, respectively. It is easily seen that when coherent phases arrive at the array, there is a large peak in the diagram. We calculate the mean of the diagram and use it as a proxy for a SNR. If the mean of the diagram is below a predetermined value, that of .5, it is considered a signal that is above the noise, otherwise the signal is not strong enough to be detected.

In order to focus our search, we construct a number of other search criteria. If a signal arrives with a high SNR ratio, we then look at the peak energy. If the peak is within a circle of radius 0.3 s/km, the time window, slowness, azimuth, and total energy is saved. A circle of radius 0.3 s/km will capture signals that arrive with an apparent horizontal velocity of at least 3 km/s, the lower bound of our discovery signals. An example of a typical coherent signal that is identified using this method is shown in Figure 11. The interesting thing to note about these signals is that the coherent energy that arrives at the array only arrives on the vertical component. No phases appear in the horizontal components of the time window.

The entire 2-year set of waveforms has been analyzed, and the results contained both local events and the signals of interest. The local events were removed by simply removing arrivals that corresponded to predicted arrivals from the CERI

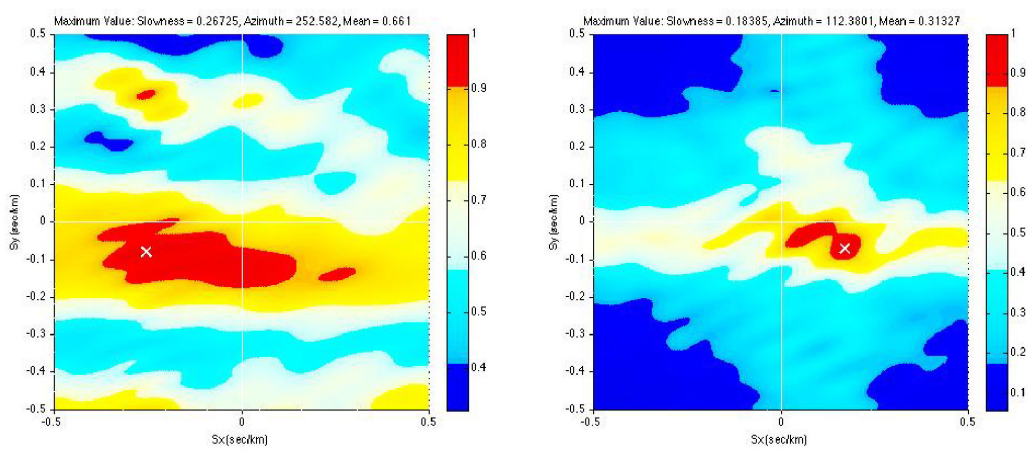

Figure 10: Above are fk-diagrams of noise (left) and an event of interest (right). Notice that the event shows a large peak while the background has many peaks at similar energy levels.

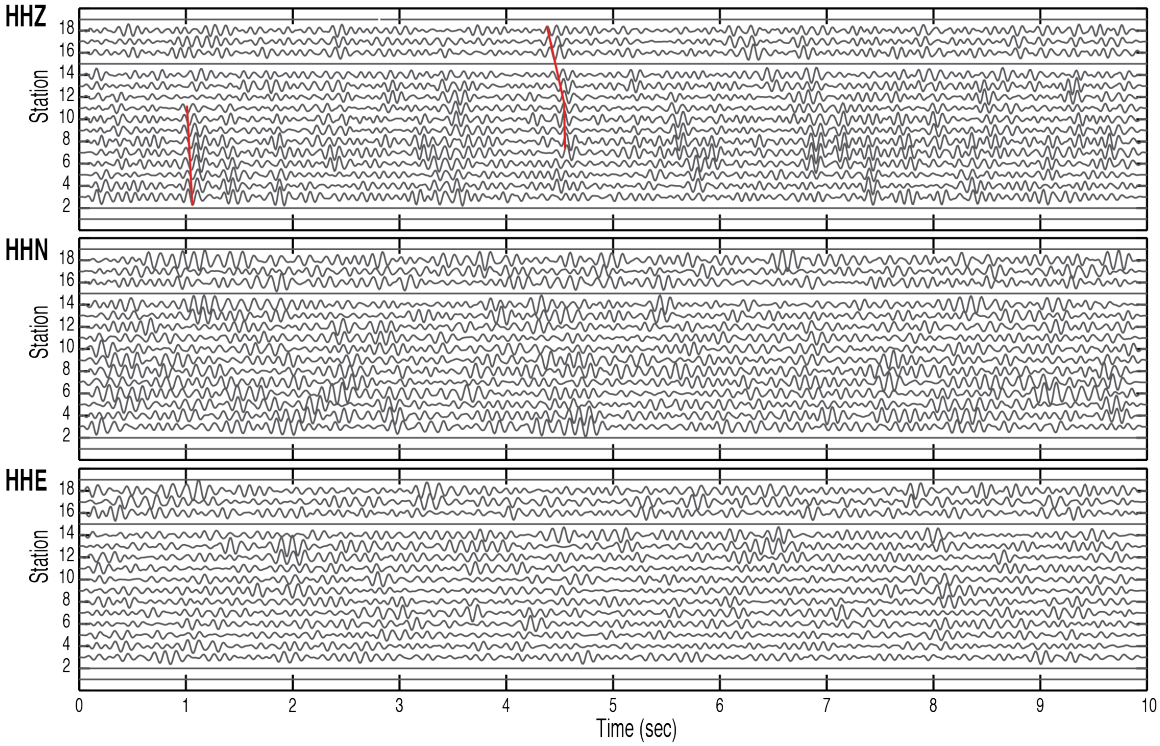

Figure 11: An example time window identified as containing a signal of interest using the algorithm. Short bursts of P-wave energy arrive at high phase velocities. Some examples are marked by red lines. These arrivals do not exhibit corresponding shear wave energy.

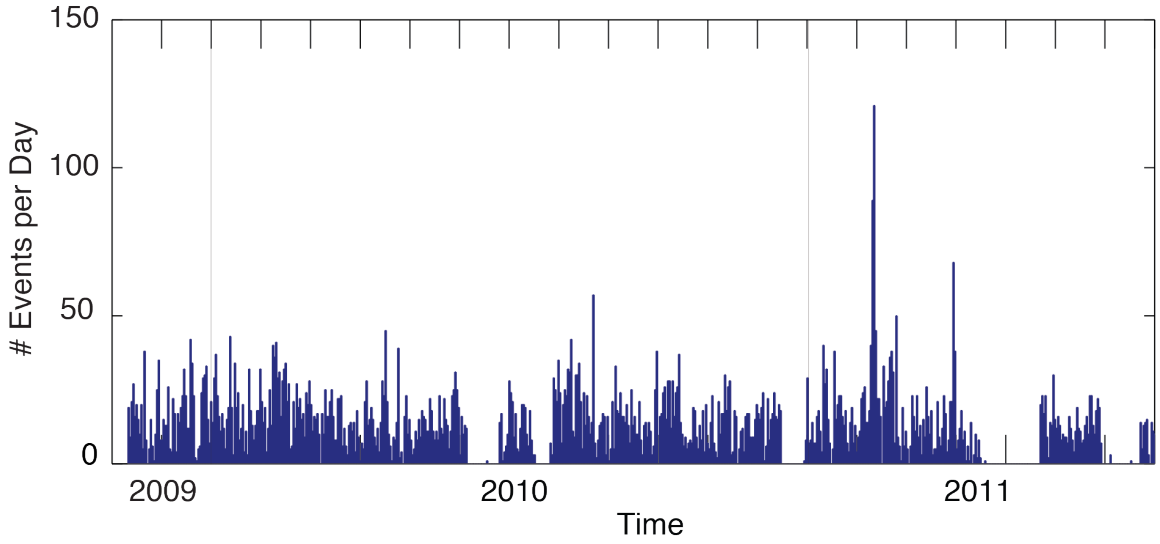

Figure 12: Final histogram showing the number of arrivals in 24 hour bins. Where available (see Figure 8), earthquakes have been removed.

catalog and other local earthquakes recorded by the array. After local events were removed, a histogram of the results was constructed (Fig. 12). Each bin represents a single 24-hour period of time starting from the beginning of the experiment till the end. There are a few anomalous features that deserve attention. First, there are five time periods that contain no data. The largest gap, around May of 2011, was during the flood of 2011. The other four gaps do not currently have such an explanation. The data was searched but no signals were detected using our detection criteria. The other anomalous portions of the data are the large spikes seen in in the spring of 2011. We are currently working on these few days as a starting point for the next portion of the study.

Another interesting result we see is from the rose graph (Fig. 13). This graph shows both direction and slowness of the incoming phases. The first thing to note is the large numbers of detections seen from the west with low slowness (or high phase velocity). A large percentage of these signals have a high apparent velocity above 3 km/s, which in agreement with what was predicted based off the discovery data set. This is strong evidence that what was seen in 2006 was not a singular event. Other large spikes that arrive, NW, SE and WSW, all agree with the seismic branches in the area.

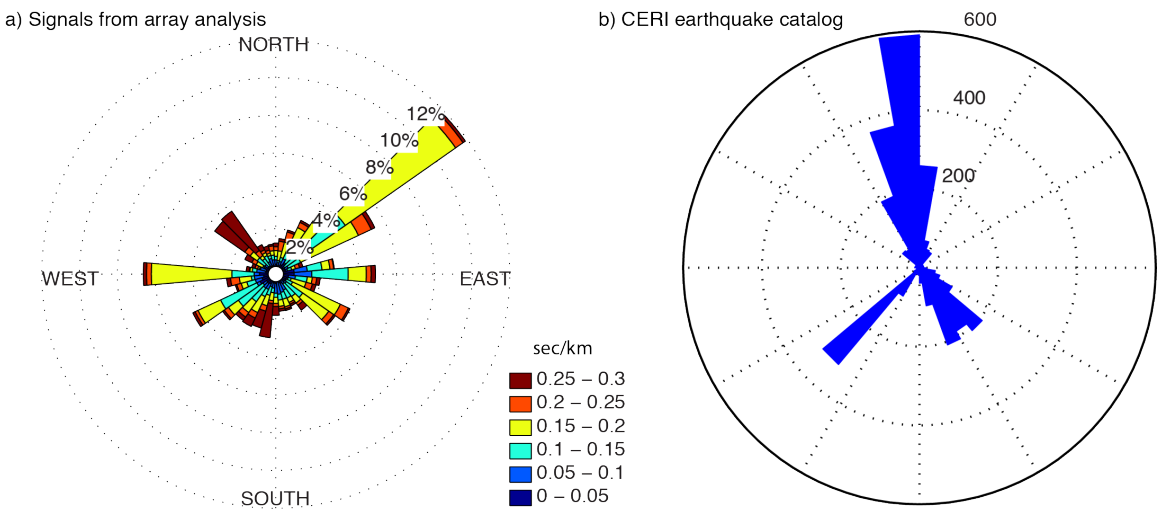

Figure 13: a) The rose graph shows the backazimuth of arriving signals and the percentage of signals that arrive within slowness bins (see legend at right, unit is sec/km). A large percentage of the signals arrive at the array with a low slowness (yellow color) coming from the west. b) Rose graph showing azimuth and number of local earthquakes recorded at the array. Only the CERI catalog is shown here. The different branches of the New Madrid seismic zone are easily identified.

The source of these signals is not yet known. In 2006, when they were originally found, they were initially interpreted as non-volcanic tremor. The results of this study show that what was seen in 2006 was not isolated, though it may not be tremor that is traditionally seen in subduction zones. These signals seem to be short bursts of P-wave like energy that arrive from directly below the array with

very high apparent horizontal velocity, at times between 25 – 28 km/sec. Most other sources of noise signals at the array arrive at surface wave velocities, ~300m/s and with P wave velocities in the sediments of about 2-2.5 km/sec The duration of signals varies greatly (Table 2). Trains, because of their slow speeds relative to seismic waves and large size, can be seen from great distances over long a period of time. Local well pumping is very periodic in nature and again, travels at slower speeds. There is a local road a few meters from the array, and as cars travel along the road, they generate large amplitude signals that are first recorded at the nearest few stations (S01-S03) traveling at surface waves speeds and then attenuate before reaching station S09 or S10. Finally, tractors moving in nearby fields are easily identified in the data. Apart from their slow surface waves, the location of the tractor can be seen at each station and can be followed as it travels from station to station.

Table 2: Noise sources and characteristics identified at the NVT array

Trains	Low velocity surface waves with long durations
Cars	Low velocity surface waves
Well Pumping	Periodic with higher frequency content, sediment P wave velocities
Tractors	Low velocity surface waves with localized source

TREMOR PROCESSING OF ARRAY & NETWORK DATA

Continuous array and networks recordings are processed for tremor using a modified version of the Brudzinski and Allen (2007) method, which is successfully used to identify tremor in Cascadia. Continuous vertical channel data is bandpass filtered between 8-15 Hz based on the frequency content preferred for FK analysis. Daytime hours are removed (05:45-18:45 CST), we apply a Hilbert transform to calculate an envelope function, smooth the envelope by averaging over 10 second windows, and decimate to a 1 sample/sec rate. We then calculate daily median nighttime amplitude. Because of the differences in instrumentation, we scale the resulting time series so that the mean nightly amplitude at each station is of the same order of magnitude as the NVT stations. Short-period network stations are multiplied by 10. HICK and PEBM are divided by 2; the remaining broadband stations are divided by 10. We then remove the median and normalize to maximum amplitude to aid in visual comparison. Data from the array is stacked prior to normalization. Figure 14 shows median nighttime amplitude at all stations sorted by distance from the NVT array.

The dominant trend at the array is higher noise levels in the winter months and lower overall noise levels in the summer months. This can also be seen on the most continuous network records (HICK, WYBT, LNXT, PEBM). We saw a similar feature in an original feasibility study aimed at applying standard subduction tremor techniques in New Madrid using only network broadband data. Using continuous

broadband data in 2009, we found a correlation in the median nightly amplitude with mean wind velocities recorded at nearby weather stations (Wiley et al., 2009).

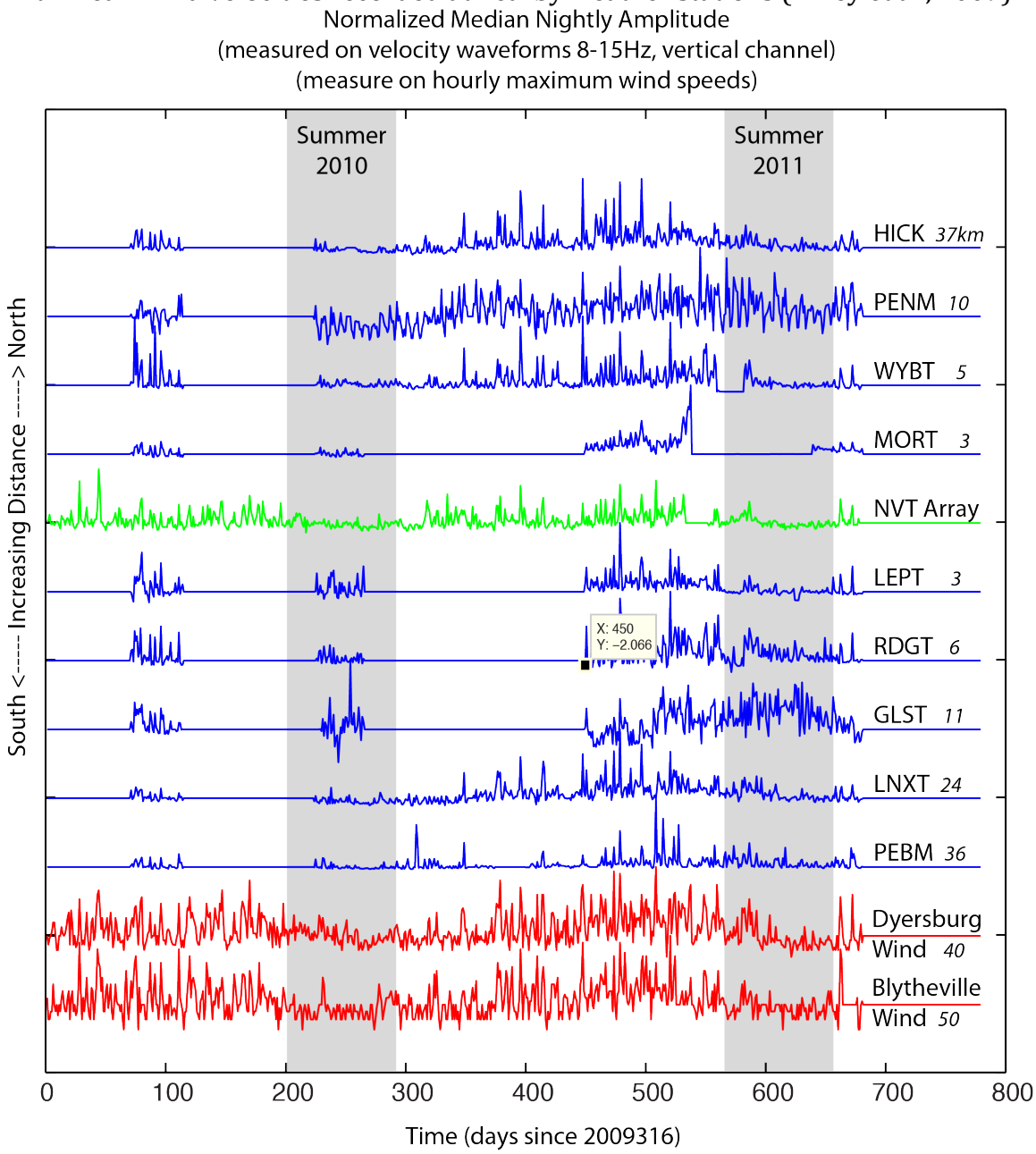

Figure 14: Median nighttime vertical channel amplitude in the 8-15 Hz frequency band. Data from the 19-station array (green) is stacked and normalized to 1. Data from the network stations (blue) is also normalized to 1. The time axis is days since 1999316 (Nov. 12, 1999). The dominant signal is low noise during summer months (defined as June-August) and a high correlation with maximum wind speeds (red).

The array and short-period/broadband network median nighttime amplitudes from late 2009-2011 also correlate well with median nightly wind speeds recorded at the Blytheville and Dyersburg NOAA climate stations (Fig. 14, red lines). For the wind

data, we take hourly maximum wind speeds as our raw data set, calculate median nighttime amplitudes, remove the median over the two-year period, and normalize to 1.

The northern Mississippi Embayment is characterized by a thick (up to 1km) layer of unconsolidated coastal plains sediment on top of bedrock. This geologic setting causes the area to be an inherently noisy environment for seismic recordings. The positive correlation between wind speed and median nightly seismic noise amplitude is likely due to wind induced tree root movement or the nearby built environment (seismic station solar panels, nearby houses, etc). Despite the fact that the seismic stations are vaulted (~3m below ground for network stations; ~1.2m for the array), tree root movement and the nearby built environment could create vibrations which travel through the sediment and cause an increase in background level seismic noise. All stations were within 500m of a significant treed area or houses, a siting issue that is hard to avoid in this largely agricultural region. Automated studies utilizing the local network or the EarthScope Transportable Array scheduled to arrive in the area in 2010-11 should expect to encounter wind induced noise fluctuations and other complications due to high cultural noise levels in this sediment basin.

What is the implication for subduction-like tremor in the New Madrid seismic zone? Along Cascadia and other margins, tremor is a sustained high noise period that spans days and dwarfs atmospheric noise signals such as wind. We do not see a similar signal in our measurements of nighttime background noise amplitude. Therefore, if there is subduction-like tremor along the Reelfoot fault, it must be very low amplitude, very short duration, occurring at frequency outside of 8-15 Hz, or (rather implausibly) only occurring during daytime hours. A low amplitude, short duration signal is certainly possible, however, and would be consistent with the discovery dataset of Langston et al. (2011).

Conclusions

A 19 element, 600m aperture phased array was successfully installed and maintained to collect a unique dataset in the New Madrid Seismic Zone. This dataset will be publicly available from the IRIS data center in September 2013 and contains teleseisms, local events, regional events, and a range of natural and man-made seismic signals. We were successful in detecting signals similar to those inferred to be possible NVT seen in a 2006 reflection experiment. These signals were impulsive, seen in the 8-15 Hz frequency band, and had phase velocities higher than 3 km/s. Further, they were only detected using the vertical components of motion. The high phase velocity and westward azimuths of a subset of these signals implies a source on the deeper parts of the Reelfoot thrust fault. Likewise, high phase velocity signals from the northeast imply sources nearly under the array. Because no S waves were detected on the horizontal channels of the array, it remains difficult to place constraints on location for these signals. It is also possible that the signals

with phase velocities lower than 6.5 km/s may have sources off the Reelfoot fault because of refraction in the basement below the unconsolidated sediments. Related processing of network broadband and short-period seismic stations do not detect these low amplitude signals but show that ambient seismic noise levels in the region correlate well with wind-induced noise.

The amplitude and polarization characteristics of these waves are not consistent with NVT observed in subduction zones or in deeper parts of the San Andreas fault. They are consistent with swarms of microseismicity at the limit of seisimic detectability. The array made it possible to detect many more earthquakes in the NMSZ than the local seismic network. We suspect that we are exploring a range of microseismicity that has not been studied before and that adequate location of these sources will need additional facilities. These facilities could include multiple phased array deployments and/or a borehole network that would allow recording within the basement Paleozoic rocks away from the noisy, near-surface unconsolidated sediments.

Students Supported/Trained

Graduate student Blaine Bockholt performed beam-forming calculations on the 19-station NVT array data, work he started as an IRIS undergraduate intern in 2010. Results will make up part of his PhD dissertation. He and fellow PhD students Lennox Thompson, Paul Ogwari, and Shishay Bisrat aided the PIs with servicing runs of the array and demobilization. Lennox Thompson also was supported under this grant and worked on completing the catalog of local events recorded by the array. Undergraduate IRIS intern Sara Wiley aided with the feasibility studies in 2009, prior to USGS funding, and Memphis Earth Science undergraduate student Eric Gamble helped complete the local earthquake catalog.

Award Bibliography to Date

Bockholt, B., C.A. Langston, H.R. DeShon (2011), Microtremors from the Reelfoot Fault, S11B-2225 presented at 2011 Spring Meeting, SSA, Memphis, TN, April.

Bockholt, B., C.A. Langston, H.R. DeShon (2011), Microtremors from the Reelfoot Fault, S11B-2225 presented at 2011 Fall Meeting, AGU, San Francisco, Calif., 5-9 Dec.

References Cited

Andrews, M. C., W. D. Mooney, and R. P. Meyer (1985). The relocation of microearthquakes in the northern Mississippi embayment, *Jour. Geophys. Res.*, *90*, 10223-10236.

Brown, J., G. Beroza, D. Shelly (2008), An autocorrelation method to detect low frequency earthquakes within tremor, *Geophys. Res. Letts.*, 35, L16305, doi:10.1029/2008GL034560.

Brudzinski, M. R., and R. M. Allen (2007). Segmentation in episodic tremor and slip all along Cascadia, *Geology, 35*, 907-910, doi:10.1130/G23740A.1

Dart, R. L., and H. S. Swolfs (1998). Contour mapping of relic structures in the Precambrian basement of the Reelfoot rift, North American midcontinent, *Tectonics*, *17*, 235-249.

Der, Z. A., R. Shumway, and A. Les (1987). Multi-channel deconvolution of *P* waves at seismic arrays, *Bull. Seism. Soc. Am.* **77,** 195–211.

Dragert, H., K. Wang, and T. S. James (2001). A silent slip event on the deeper Cascadia subduction interface, *Science*, *292*, 1525-1528.

Eagar, K. C., G. L. Pavlis, and M. W. Hamburger (2006). Evidence of possible induced seismicity in the Wabash Valley Seismic Zone from improved microearthquake locations, *Bull. Seism. Soc. Amer*, 96, 1718-1728, doi:10.1785/0120050190.

Ervin, C. P., and L. D. McGinnis (1975). Reelfoot rift: Reactivated pre- cursor to the Mississippi embayment, *Geol. Soc. Am. Bull.*, *86*, 1,287-281,295.

Forte, A. M., J. X. Mitrovica, R. Moucha, N. A. Simmons, and S. P. Grand (2007). Descent of the ancient Farallon slab drives localized mantle flow below the New Madrid seismic zone, *Geophys. Res. Lett.*, *34*, doi:10.1029/2006GL027895.

Ghosh A, Vidale JE, Peng ZG, et al. (2009), Complex nonvolcanic tremor near Parkfield, California, triggered by the great 2004 Sumatra earthquake, *J. Geophys. Res.*, 114, B00A15.

Jemberie, A.L., and C.A. Langston (2005). Site Amplification, scattering and intrinsic attenuation in the Mississippi embayment from coda waves, *Bull. Seism. Soc. Am., 95,* 1716-1730.

Langston, C. A. (2003). Local Earthquake Wave Propagation Through Mississippi Embayment Sediments: I. Body Wave Phases and Local Site Responses, *Bull. Seism. Soc. Am.*, *93*, 2664-2684.

Langston, C.A. D.M. Rieger, and M.B. Magnani (2010), Unusual Microseisms Seen in the Reelfoot Fault Zone, Northern Tennessee, from a Reflection Experiment, *Bull. Seism. Soc. Am.*, 100, 377-383.

Langston, C. A., P. Bodin, C. Powell, M. Withers, S. Horton, and W. Mooney (2005). Bulk sediment Qp and Qs in the Mississippi embayment, Central U.S., *Bull. Seism. Soc. Am.*, *95*, 2162-2179.

Langston, C. A., P. Bodin, C. Powell, M. Withers, S. Horton, and W. Mooney (2006). Explosion source strong ground motions in the Mississippi embayment, *Bull. Seism. Soc. Am.*, *96*, 1038-1054.

Liu, Y., and J. R. Rice (2005), Aseismic slip transients emerge spontaneously in three-dimensional rate and state modeling of subduction earthquake sequences, *J. Geophys. Res.*, 110, B08307, doi:10.1029/2004JB003424.

Liu, Y.J. and J.R. Rice (2007), Spontaneous and triggered aseismic deformation transients in a Subduction fault model, *J. Geophys. Res.*, 112, B09404, doi:10.1029/2007JB004930.

Maceira M, Rowe CA, Beroza G, et al. (2010), Identification of low-frequency earthquakes in non-volcanic tremor using the subspace detector method, *Geophys. Res. Letts.*, 37, L06303.

Nadeau, R. M., and D. Dolenc (2005). Nonvolcanic tremors deep beneath the San Andreas Fault, *Science*, *307*, 389.

Nakata R, Suda N, Tsuruoka H (2008), Non-volcanic tremor resulting from the combined effect of Earth tides and slow slip events, *Nature Geosci.*, 1, 676-678.

Obara, K. (2002). Nonvolcanic deep tremor associated with subduction in southwest Japan, *Science*, *296*, 1679.

Pavlis, G. L., F. L. Vernon, D. Harvey, and D. Quinlan (2004). The generalized earthquake location (GENLOC) package: A modern earthquake location library, *Computers in Geosciences,* 30, 1079-1091.

Peng ZG, Chao KV (2008), Non-volcanic tremor beneath the Central Range in Taiwan triggered by the 2001 M-w 7.8 Kunlun earthquake, *Geophys. J. Int.*, 175, 825-829.

Peng ZG, Vidale JE, Creager KC, et al. (2008), Strong tremor near Parkfield, CA, excited by the 2002 Denali Fault earthquake, *Geophys. Res. Letts.*, 35, L23305.

Peng ZG, Vidale JE, Wech AG, et al., (2009), Remote triggering of tremor along the San Andreas Fault in central California, *J. Geophsy. Res.*, 114, B00A06.

Rogers, G., and H. Dragert (2003). Episodic tremor and slip on the Cascadia subduction zone: the chatter of silent slip, *Science*, *300*, 1942-1943.

Rubinstein JL, Vidale JE, Gomberg J, et al. (2007), Non-volcanic tremor driven by large transient shear stresses, *Nature*, 448, 579-582.

Rubinstein JL, La Rocca M, Vidale JE, et al. (2008), Tidal modulation of nonvolcanic tremor, *Science*, 319, 186-189.

Scholz, C.H. (1998), Earthquakes and friction laws, *Nature, 391*, 37-42.

Schwartz, S. Y., and J. M. Rokosky (2007), Slow slip events and seismic tremor at circum-pacific subduction zones, *Rev. Geophys*., 45, RG3004, doi:10.1029/2006RG000208.

Shelly DR, (2010), Migrating tremors illuminate complex deformation beneath the seismogenic San Andreas fault, *Nature*, 463, 648-U75.

Shelly, D. R., G. C. Beroza, S. Ide, and S. Nakamula (2006), Lowfrequency earthquakes in Shikoku, Japan and their relationship to episodic tremor and slip, *Nature*, 442, 188–191.

Stearns, R. G. (1957). Cretaceous, Paleocene, and lower Eocene geologic history of the northern Mississippi embayment, *Geol. Soc. Am. Bull.*, *68*, 1077-1100.

Stearns, R. G., and M. V. Marcher (1962). Late Cretaceous and subsequent structural development of the northern Mississippi embayment area, *Geol. Soc. Am. Bull.*, *73*, 1387-1394.

Thomas, W. A. (2006). Tectonic inheritance at a continental margin, *GSA Today*, *16*, doi: 10.1130/1052-5173.

Thomas AM, Nadeau RM, Burgmann R (2009), Tremor-tide correlations and near-lithostatic pore pressure on the deep San Andreas fault, *Nature*, 462, 1048-U105.

Wech, A. G., and K. C. Creager (2007). Cascadia tremor polarization evidence for plate interface slip, Geophys. Res. Let., 34, L22306, doi:10.1029/2007GL031167.